Supplementary Material of OID: Outlier Identifying and Discarding in Blind Image Deblurring

Liang Chen[1], Faming Fang[1] ⋆, Jiawei Zhang[2], Jun Liu[3], and Guixu Zhang[1]

[1] Shanghai Key Laboratory of Multidimensional Information Processing, East China Normal University
[2] SenseTime Research
[3] Northeast Normal University
{liangchen527, zhjw1988}@gmail.com,
{fmfang, gxzhang}@cs.ecnu.edu.cn, liuj292@nenu.edu.cn

In this supplementary material, we provide,
1. More analysis of the proposed method;
2. More experimental results.

1 Further Analysis

In this section, we first analysis some detail settings of the proposed model. We then use the proposed framework to extend some potential non-blind deblurring methods, and we further discuss the effectiveness of the method which includes both the blind and non-blind steps. At the end of this section, we give a possible extension of the proposed non-blind method.

1.1 Running time comparisons

We further compare OID with other blind deblurring methods on blurry images with different sizes in term of running times. As is shown in Table 1, OID performs favorably against recent outlier handling methods [4, 14], and it also conducts one of the fastest running time among recent optimization-based methods.

Table 1. Running time comparison for different sizes of blurry image (seconds). All methods are implemented in MATLAB.

Methods / size	Xu et al. [19]	Zhong et al. [21]	Pan et al. [14] (outlier)	Pan et al. [15] (dark)	Dong et al. [4]	Gong et al. [6][4]	Chen et al. [1]	Ours
255×255	2.71	12.40	154.75	137.43	155.96	180.00	65.20	56.83
600×600	16.89	53.19	662.32	945.91	736.68	∞	376.94	252.07
800×800	31.14	77.55	1113.12	1992.44	1214.17	∞	755.43	437.86

.

1.2 Parameter settings

In this subsection, we analyse the parameters that affect outlier detecting process (i.e., α and β in Eq. (9) of the paper). These two parameters control the reasonable range of

⋆ Corresponding Author

[4] The code from [6] is not provided, we use the reported processing time in their paper (hardware settings are similar).

$B_i - (I \otimes K)_i$ and the range of corresponding weight W_i. Because the range of weight is fixed as default setting (i.e., $W_i \in (0, 1)$), we only consider the range of $B_i - (I \otimes K)_i$. As shown in Fig. 1, when the range is too narrow (blue line in Fig. 1 (a)), many inliers are also assigned with small weights (Fig. 1 (h)), which results in less details in the recovered image (Fig. 1 (d)); and when the range is too wide (red line in Fig. 1 (a)), outliers can not be fully detected (Fig. 1 (e) and (h)); and we found parameters using our settings can better detect outliers while keeping inliers (Fig. 1 (f) and (i)).

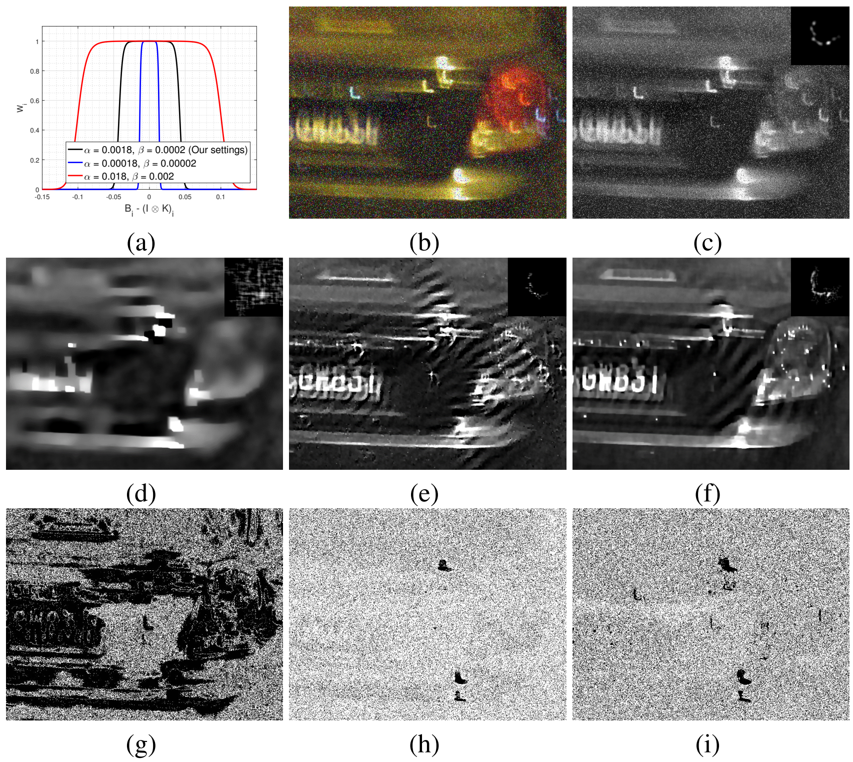

Fig. 1. (a) Visualization of Eq. (9) of the paper with different parameter settings. (b) Blurry image. (c) Input blurry image and kernel for final pyramid, the kernel is generated from previous coarse pyramids. (d)-(f) Latent images and blur kernels using different parameter settings (correspond to blue, red, black lines in (a) from left to right). (g)-(i) Corresponding weight maps for latent image of (d)-(f). Our proposed parameter settings can best discard outliers while keeping inliers.

1.3 Sparse constraint on outliers

As mentioned in section 2 in the main manuscript, the l_1 norm constraint on outliers ($\overline{W}$) is not the only option. We here compare it with l_0 constraint on outliers. We do not consider the p-norm ($0 < p < 1$) sparse constraint since it does not lead to a close-form solution of corresponding weight entry. With l_0 imposed on outliers, Eq. (3) of the paper is modified into,

$$\begin{gathered}\min_{I,K,W}\sum_i W_i|B_i-(I\otimes K)_i|^2+\lambda\|\nabla I\|_{0.8}+\theta\|K\|_2^2+\alpha\|\overline{W}\|_0+\beta\sum_i(W_i\log W_i+\overline{W_i}\log\overline{W_i}),\\ \text{s.t.}\quad W_i+\overline{W_i}=1,\qquad\left\{W_i,\overline{W_i}\right\}\in[0,1],\end{gathered}\tag{1}$$

we here define $0*\log 0=0$. Thus the updating refer to weighting matrix turns into,

$$\begin{gathered}\min_{W,\overline{W}}\sum_i W_i|B_i-(I\otimes K)_i|^2+\alpha\|\overline{W}\|_0+\beta\sum_i(W_i\log W_i+\overline{W_i}\log\overline{W_i}),\\ \text{s.t.}\quad W_i+\overline{W_i}=1,\qquad\left\{W_i,\overline{W_i}\right\}\in[0,1].\end{gathered}\tag{2}$$

We use the same strategy in the main manuscript by decomposing Eq. (2) into sub-problems, and the energy is given by,

$$\min_{W_i}E(W_i)=\min_{W_i}W_i|B_i-(I\otimes K)_i|^2+\alpha|1-W_i|^0+\beta(W_i\log W_i+(1-W_i)\log(1-W_i)).\tag{3}$$

We have the closed-form solution of W_i,

$$W_i=\begin{cases}(\exp(\frac{|B_i-(I\otimes K)_i|^2}{\beta})+1)^{-1}, & E(W_i)<E(1)=|B_i-(I\otimes K)_i|^2,\\ 1, & \text{otherwise.}\end{cases}\tag{4}$$

The form of W_i imposed on different sparse constraints are shown in Fig. 2 (a). As shown in the figure, when the parameters are the same, the curve of l_0 acts as a hard threshold, and the differences between l_1 and l_0 curves are subtle. We also compare with the case without sparse constraint (i.e., $\alpha=0$). We use the same example in Fig. 1 (b), as shown in Fig. 3 (a)-(f). We can see the results generated by l_1 or l_0 constraints are similar, while without sparse constraint is less effective. A thorough experiment on our dataset is demonstrated in Fig. 2 (b). The ultimate results are close (with average PSNR values for l_1, l_0 and without sparse constraints are 30.01, 29.96 and 23.51, respectively).

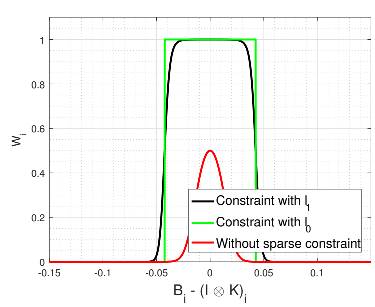

(a)

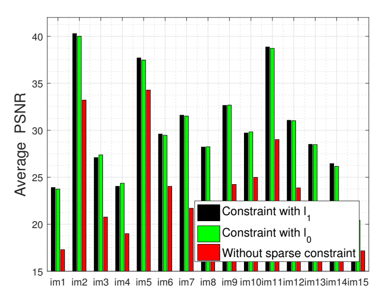

(b)

Fig. 2. (a) Visualization of weight map under different constraints. (b) PSNR values of our dataset under different sparse constraints.

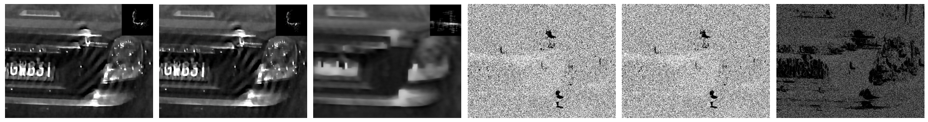

(a) (b) (c) (d) (e) (f)

Fig. 3. (a)-(c) are latent images and kernels with l_1, l_0 and without sparse constraints. (d)-(f) are corresponding weight maps for latent image of (a)-(c).

1.4 Limitation and future work

Although OID is able to deblur blurry images with significant outliers, we find one of its limitations is that it is ineffective in handling blurry images with severe Gaussian noise. As shown in Fig. 4, OID fails to recover sharp images. Moreover, recent outlier deblurring methods, which assume outliers do not follow the linear formation rule, are all invalid in this occasion. The results indicate that Gaussian noise can not be treated as outliers like non-Gaussian noise. Our future work aims to develop a more robust model that can handle both significant Gaussian and non-Gaussian noise.

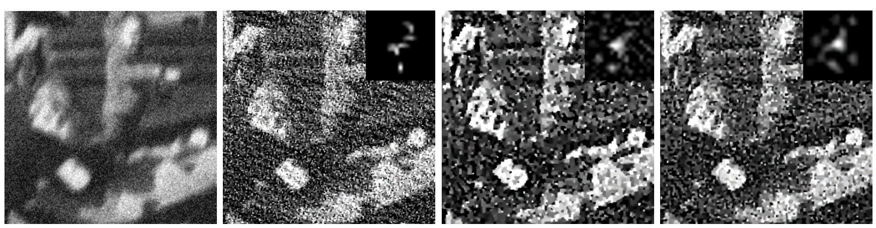

(a) Input (b) Dong et al. [4] (c) Pan et al. [14] (d) Ours

Fig. 4. Blind deblurring results of a blurry image contaminated with severe Gaussian noise with noise density of 0.1. Recent outlier deblurring methods are not able to handle this situation.

1.5 Recovering missing information with the proposed non-blind deblurring method

As introduced in [3], pixels in blurred images contain partial information of its neighboring pixels due to the scattering nature of blur. Thus, outlier pixels can still be reconstructed if the neighboring region contains enough information about it, although outliers do not contribute to the recovering process in this case. To verify the effectiveness of our non-blind method on recovering missing information, we conduct an experiment shown in Fig. 5. We add outliers of different intensities and sizes to a blurry image with known blur kernel. The deblurrin results demonstrate that, OID can robustly recover blurry images contaminated by small outliers. For large outliers, these pixels can only be smoothed out. Moreover, OID consistently outperforms the methods from [3, 14].

(a) Input (b) W/O outlier handling (c) Cho et al. [3] (c) Pan et al. [14] (d) Ours (e) GT

Fig. 5. Recovering a blurry image with missing information [3]. Here the values of the quadrangles are 1, 0.5 and 0, respectively. Best viewed on high-resolution displays with zoom-in.

1.6 Effectiveness of the proposed algorithm

We first analyse the effectiveness of different blind deblurring methods using examples with different densities of outliers. As shown in Fig. 6. OID performs robust when facing different densities of outliers, while methods from [4,14] and the extension of [3] is ineffective facing heavy outliers.

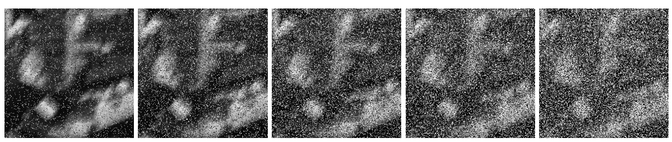

(a) Blurry images with increasing densities of outliers ($10\% - 50\%$ from left to right).

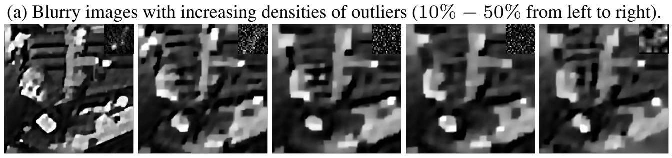

(b) Results from Pan et al. [14]

(b) Results from Dong et al. [4]

(b) Results from the extension of Cho et al. [3]

(b) Results of OID

Fig. 6. Deblurring results of blurry images with increasing densities of outliers.

An example with multiple outliers is shown in Fig. 7. Note that outliers detected by OID are more precise than that by the extension of [3] over iterations, which leads to a more clearer image. The final results validates the superiority of the proposed latent image updating strategy.

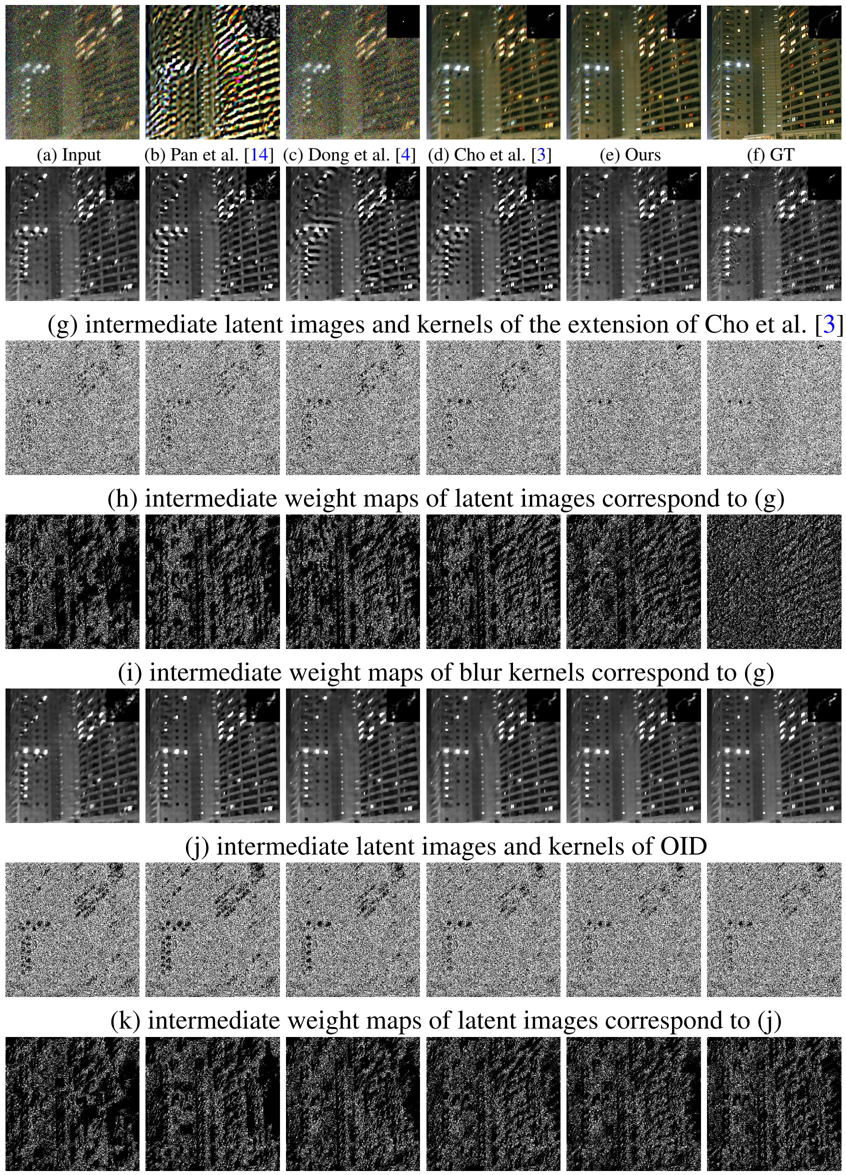

(a) Input (b) Pan et al. [14] (c) Dong et al. [4] (d) Cho et al. [3] (e) Ours (f) GT

(g) intermediate latent images and kernels of the extension of Cho et al. [3]

(h) intermediate weight maps of latent images correspond to (g)

(i) intermediate weight maps of blur kernels correspond to (g)

(j) intermediate latent images and kernels of OID

(k) intermediate weight maps of latent images correspond to (j)

(l) intermediate weight maps of blur kernels correspond to (j)

Fig. 7. Comparison with several outlier handling methods.

Our non-blind deblurring method is a direct extension of the proposed blind deblurring method. To demonstrate the effectiveness of our non-blind deblurring method, we compare it with state-of-the-art outlier handling methods [3, 14] on dataset [10] with increasing impulsive noise. As shown in Fig. 8, OID performs more robust than [3, 14]. Examples are shown in Fig. 9;

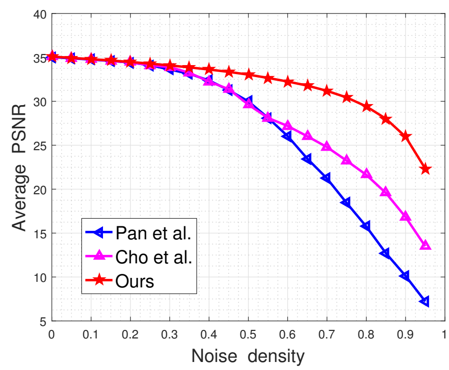

Fig. 8. Quantitative evaluation of our non-blind method and other robust non-blind methods [3, 14] on the dataset [10] with increasing impulsive noise (density from 0 to 0.95).

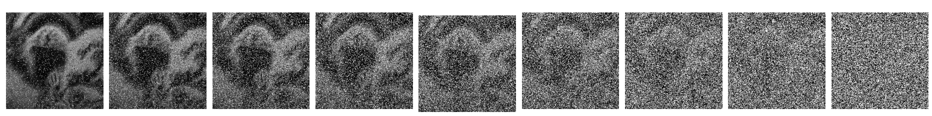

(a) Examples with increasing noise (density from 0.1 to 0.9)

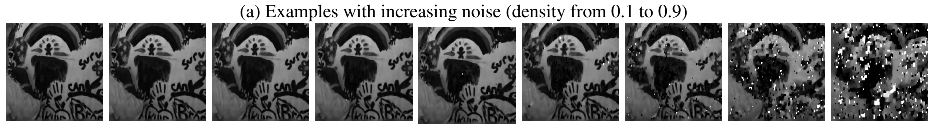

(b) Results of [14]. PSNR values (left to right) are 37.17, 36.94, 36.77, 33.55, 29.21, 24.46, 19.62, 13.84, 10.03.

(c) Results of [3]. PSNR values (left to right) are 37.28, 37.07, 36.87, 33.56, 29.87, 26.33, 24.12, 21.36, 16.61.

(d) Our results. PSNR values (left to right) are 37.28, 37.08, 36.89, 36.58, 36.05, 35.20, 33.75, 30.92, 25.59.

Fig. 9. Comparison of several non-blind deblurring methods with blurry images contaminated by significant impulsive noise.

1.7 Comparisons of OID conducted on different image scales

As depicted in the manuscript, the proposed algorithm is implemented in a coarse-to-fine manner, while OID is only conducted in the finest image pyramid for the sake of efficiency [21]. Questions may be raised whether it will benefit the algorithm if OID is conducted from the first to the last image scale. We use examples to examine the effectiveness of different strategies. As shown in Fig. 10, differences between results generate with these two strategies are subtle, while the processing time with OID conducted on all image pyramids is greater than that on the last pyramid. We further use the benchmark dataset (from Levin et al. [10]) with 10% density of outliers to verify the difference of these two schemes. Average PSNR for OID conducted on all image pyramids is 29.179, and the corresponding result for OID conducted on the last image pyramid is 29.183. The overall results show that conduct OID in all image pyramids is not necessary.

(a) Input

(b) PSNR: 23.71
Running time: 512.99 s

(c) PSNR: 23.69
Running time: 301.80 s

(d) Input

(e) PSNR: 25.50
Running time: 353.81 s

(f) PSNR: 25.51
Running time: 205.79 s

Fig. 10. Comparisons of OID conducted on different image scales. (b) and (e) are results of OID conducted on all image scales. (c) and (f) are results of OID conducted on the finest image scale.

Table 2. Comparison on the dataset with impulse noise in terms of average PSNR and SSIM.

	Cho and Lee [2]	Xu and Jia [18]	Xu et al. [19]	Zhong et al. [21]	Pan et al. [14]	Dong et al. [4]	Ours	GT kernels
PSNR	21.81	18.77	24.39	24.10	25.95	28.03	30.01	32.92
SSIM	0.5926	0.5464	0.6778	0.6860	0.7654	0.7983	0.8469	0.8993

2 Further comparison

In this section, we first provide detail comparison results on our dataset with impulsive noise (details and results about other used datasets can be found in the main manuscript), dataset with saturated images [13] and the dataset without outliers [10], then we show more comparison examples against state-of-the-art methods.

As shown in Fig. 11, our dataset consists of 15 800×800 sharp images and 8 blur kernels from [10]. We add the impulse noise (as it is one of the most common non-Gaussian noise) to each image. The noise density is set to be 0.1. Average SSIM and PSNR values are shown in Table 2. PSNR values from different methods of each image are shown in Fig. 12. OID consistently outperforms state-of-the-art methods [2, 4, 14, 18, 19, 21]. Access to the ground truth data will be released soon.

Fig. 11. Images and kernels we used to generate our dataset.

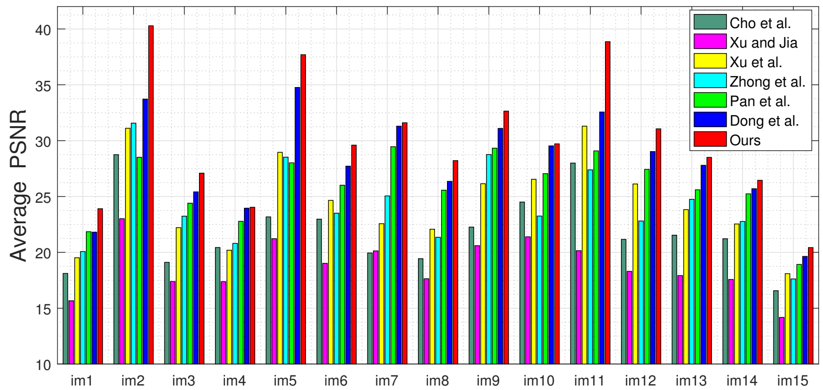

Fig. 12. Quantitative evaluation on the proposed dataset with impulsive noise.

We also test OID on an provided dataset with saturated images [13]. We show the average SSIM values of state-of-the-art methods in Table 3 (average PSNR values are presented in the manuscript). As depicted in the table, OID leads among state-of-the-art methods.

Table 3. Comparison on the dataset with saturated pixels [13] in term of average SSIM.

	Cho and Lee [2]	Xu et al. [19]	Pan et al. [13] (text)	Chen et al. [1]	Pan et al. [14] (outlier)	Dong et al. [4]	Ours	GT kernels
SSIM	0.6860	0.8149	0.7609	0.8108	0.8407	0.8269	0.8456	0.8717

OID is also effective with images without outliers. Beside the dataset provided in [8], we also test OID on a benchmark dataset provided by Levin et al. [10]. The average PSNR values are presented in Table 4. Our model performs favorably among state-of-the-art methods. The results illustrate the effectiveness of the proposed method.

Table 4. Quantitative evaluation on the dataset [10] without outliers in term of average PSNR.

	Fergus et al. [5]	Shan et al. [16]	Xu and Jia [18]	Krishnan et al. [9]	Cho and Lee [2]	Xu et al. [19]	Pan et al. [13]	Yan et al. [20]	Dong et al. [4]	Ours
PSNR	29.46	30.68	30.75	29.04	30.79	30.86	30.35	32.27	31.78	32.34

2.1 More comparison examples

We show more comparison results by OID and the state-of-the-art methods. Results are directly provided by the authors using default parameters. We use the same parameter settings in all experiments.

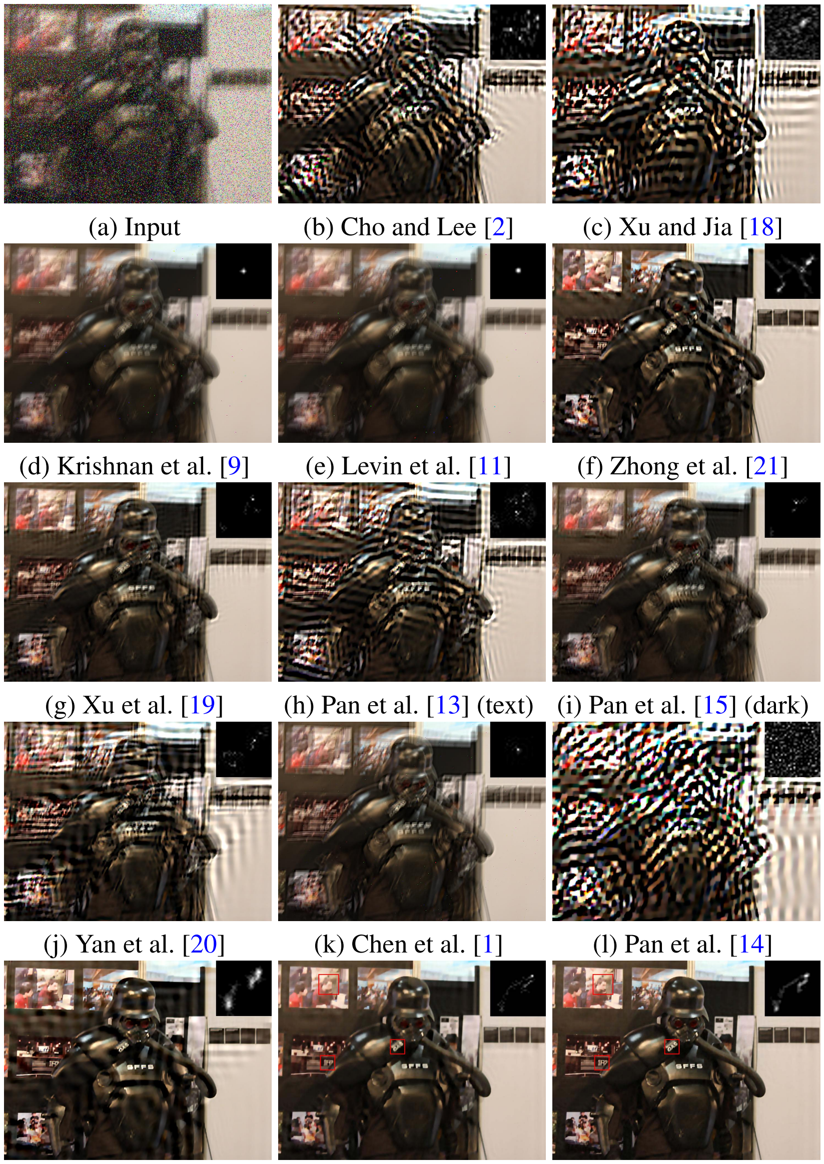

(a) Input (b) Cho and Lee [2] (c) Xu and Jia [18]

(d) Krishnan et al. [9] (e) Levin et al. [11] (f) Zhong et al. [21]

(g) Xu et al. [19] (h) Pan et al. [13] (text) (i) Pan et al. [15] (dark)

(j) Yan et al. [20] (k) Chen et al. [1] (l) Pan et al. [14]

(m) Dong et al. [4] (n) Extension of [3] (o) Ours

Fig. 13. Blurry image with impulsive noise. Here we use our non-blind deblurring method after kernels are acquired. Results generated by OID contain less artifacts and more textures. Also note that the extension of [3] generates results with less sharp details than ours as shown in the red boxes.

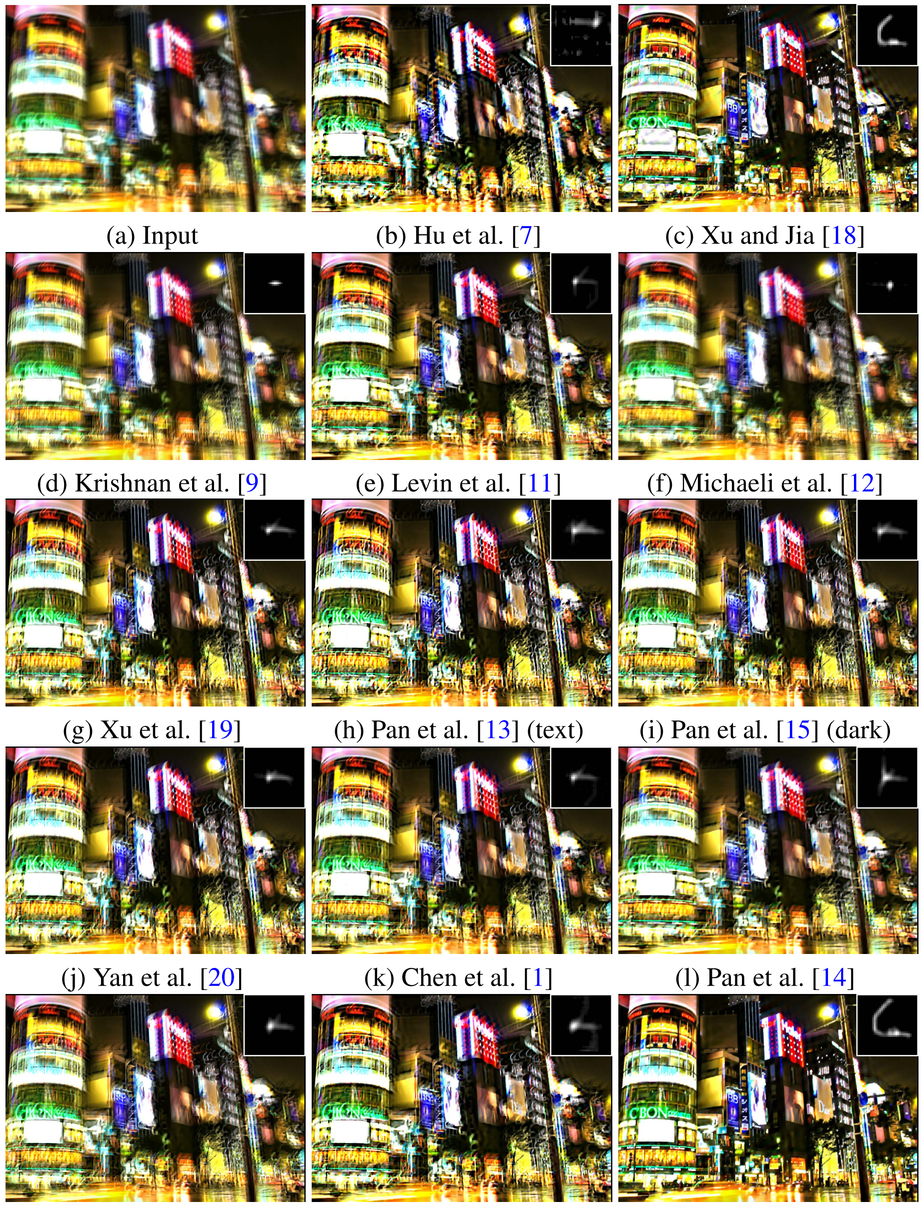

(a) Input (b) Hu et al. [7] (c) Xu and Jia [18]

(d) Krishnan et al. [9] (e) Levin et al. [11] (f) Michaeli et al. [12]

(g) Xu et al. [19] (h) Pan et al. [13] (text) (i) Pan et al. [15] (dark)

(j) Yan et al. [20] (k) Chen et al. [1] (l) Pan et al. [14]

(m) Dong et al. [4] (n) Extension of [3] (o) Ours

Fig. 14. Blurry image with saturated regions. Here we use our non-blind deblurring method after kernels are acquired. Results generated by OID contain clearer details.

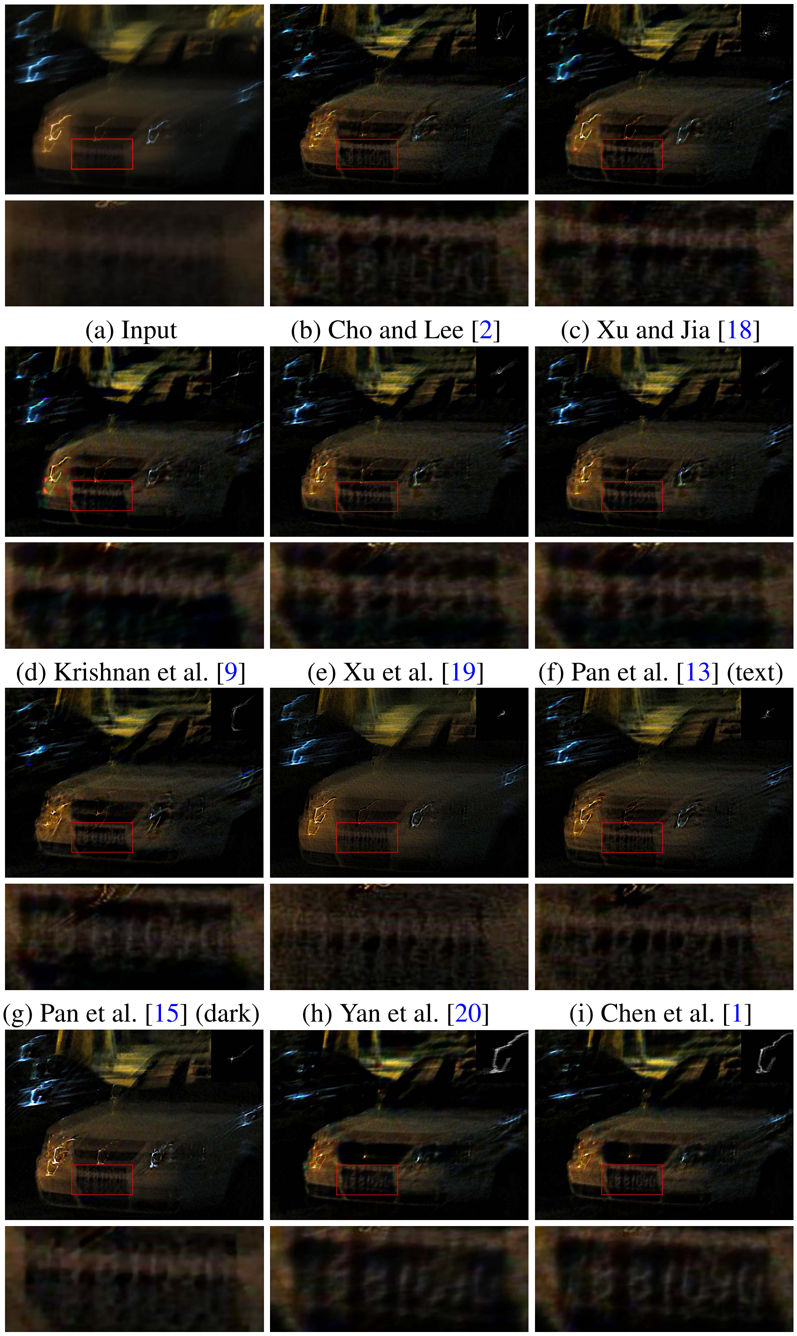

(a) Input (b) Cho and Lee [2] (c) Xu and Jia [18]

(d) Krishnan et al. [9] (e) Xu et al. [19] (f) Pan et al. [13] (text)

(g) Pan et al. [15] (dark) (h) Yan et al. [20] (i) Chen et al. [1]

(j) Pan et al. [14] (k) Dong et al. [4] (l) Ours

Fig. 18. Real-world blurry image with saturated pixels. Here we use the same non-blind deblurring method [17] after kernels are acquired. OID generates comparable results with shaper edges than the outlier handling methods [4, 14] (better viewed on high resolution with zoom-in).

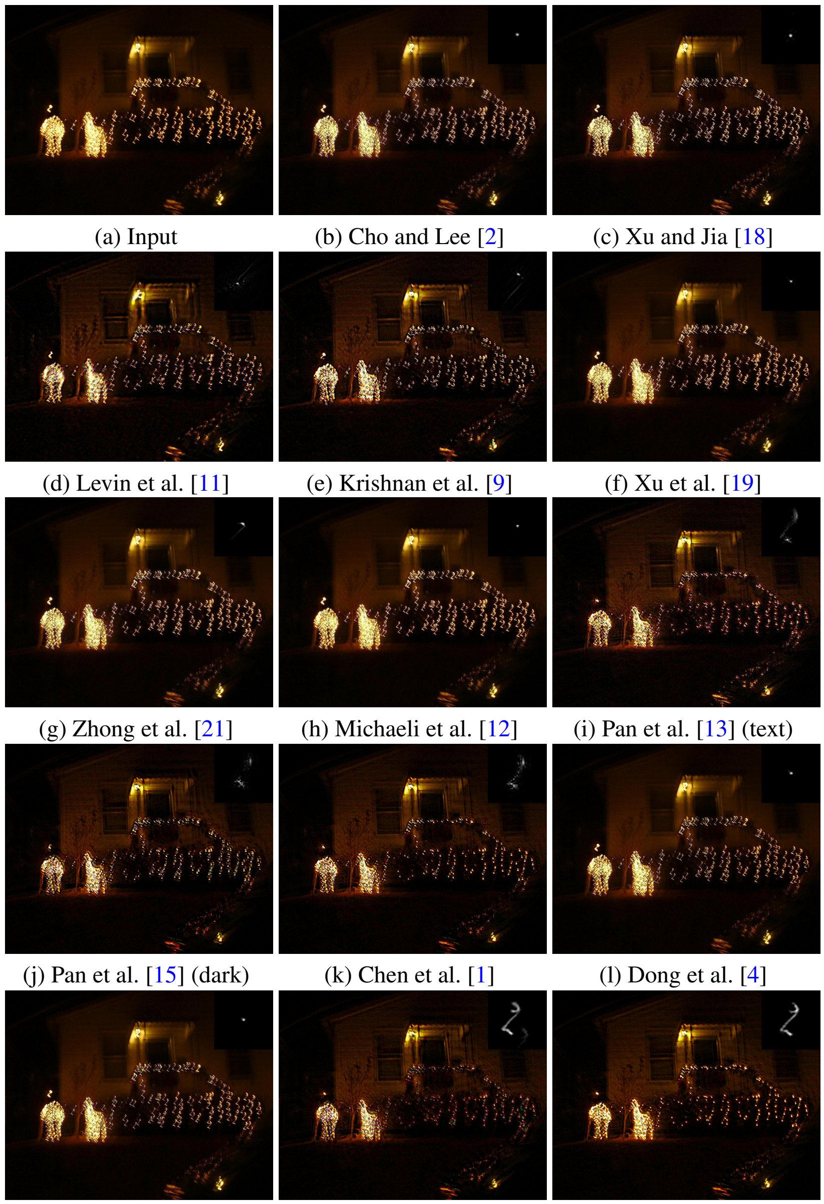

(a) Input (b) Cho and Lee [2] (c) Xu and Jia [18]
(d) Levin et al. [11] (e) Krishnan et al. [9] (f) Xu et al. [19]
(g) Zhong et al. [21] (h) Michaeli et al. [12] (i) Pan et al. [13] (text)
(j) Pan et al. [15] (dark) (k) Chen et al. [1] (l) Dong et al. [4]
(m) Pan et al. [14] (n) Hu et al. [7] (o) Ours

Fig. 15. Real-world blurry image with saturated pixels. Here we use the same non-blind deblurring method [17] after kernels are acquired. OID generates a more accurate blur kernel. Please zoom-in for a better view.

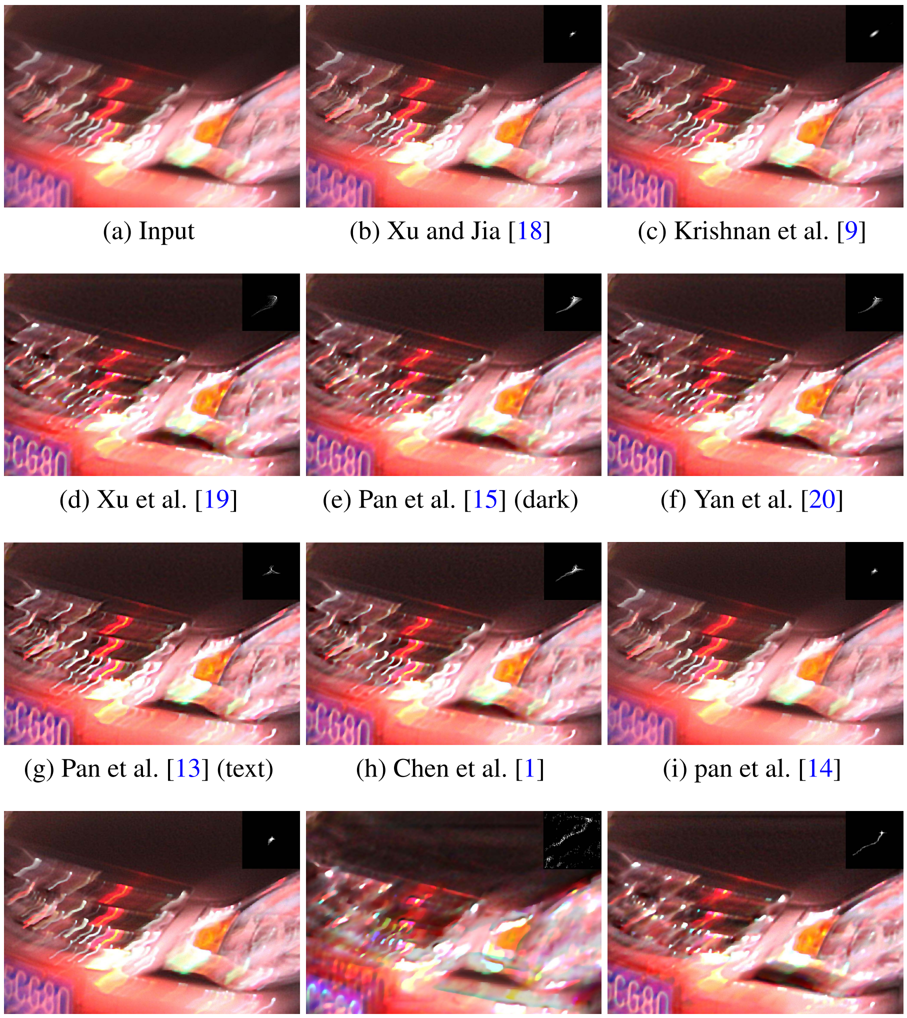

(a) Input (b) Xu and Jia [18] (c) Krishnan et al. [9]

(d) Xu et al. [19] (e) Pan et al. [15] (dark) (f) Yan et al. [20]

(g) Pan et al. [13] (text) (h) Chen et al. [1] (i) pan et al. [14]

(j) Dong et al. [4] (k) Hu et al. [7] (l) Ours

Fig. 16. Real-world blurry image with massive saturated pixels. Here we use the same non-blind deblurring method [7] after kernels are acquired. OID generates a more accurate blur kernel. Please zoom-in for a better view.

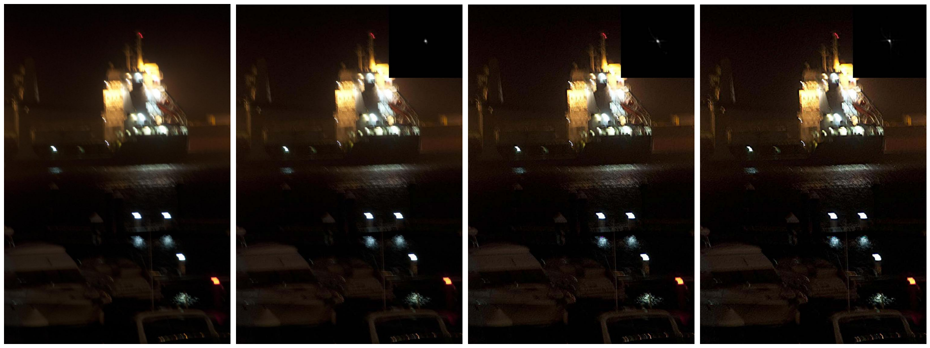

(a) Input (b) Cho and Lee [2] (c) Xu and Jia [18] (d) Krishnan et al. [9]

(e) Xu et al. [19] (f) Michaeli et al. [12] (g) Yan et al. [20] (h) Chen et al. [1]

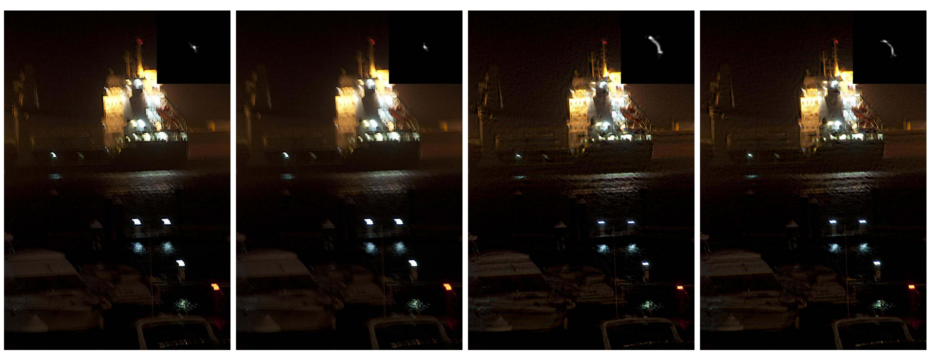

(i) Pan et al. [14] (j) Dong et al. [4] (k) Hu et al. [7] (l) Ours

Fig. 17. Real-world blurry image with saturated pixels. Here we use the same non-blind deblurring method [17] after kernels are acquired. State-of-the-art methods fail to estimate correct kernels in this situation, including recent outlier handling methods [4, 14]. Moreover, kernel estimated by OID is visually similar to that of [7], and from which the light streak is manually extracted.

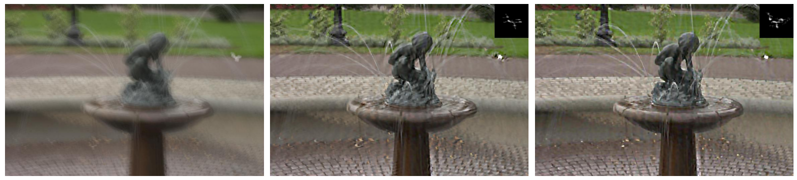

(a) Input (b) Fergus et al. [5] (c) Ours

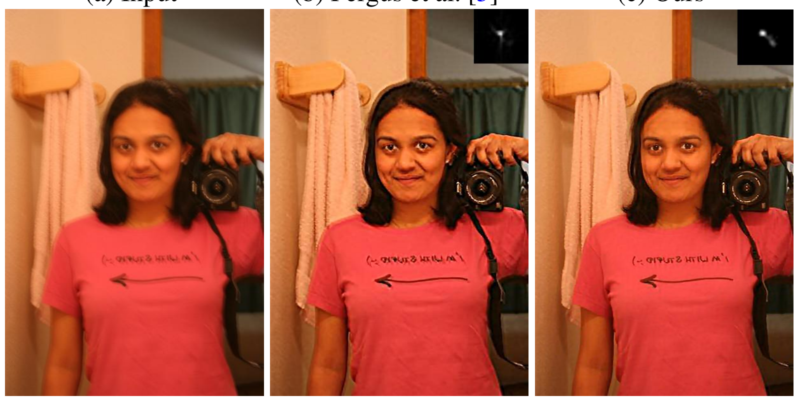

(d) Input (e) Krishnan et al. [9] (f) Ours

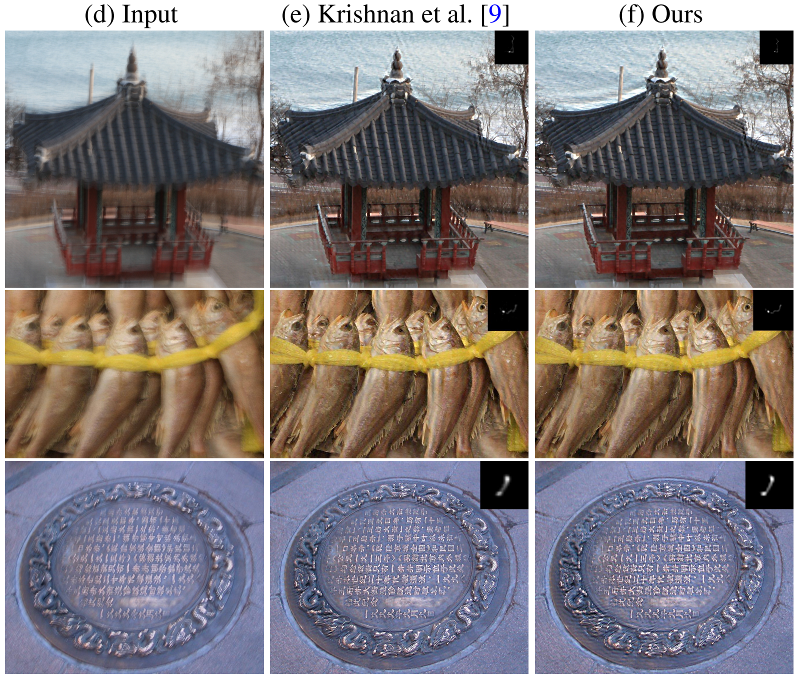

(g) Input (h) Cho and Lee [2] (i) Ours

Fig. 19. Comparison with state-of-the-art methods on real-world examples, OID performs comparable or even better than these methods.

(a) Input (b) Shan et al. [16] (c) Ours

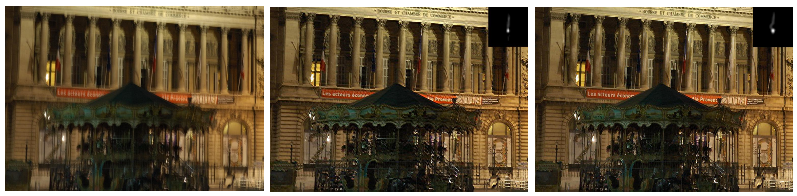

(d) Input (e) Xu and Jia [18] (f) Ours

(g) Input (h) Xu et al. [19] (i) Ours

(j) Input (k) Zhong et al. [21] (l) Ours

Fig. 20. Comparison with state-of-the-art methods on real-world examples, OID performs comparable or even better than these methods.

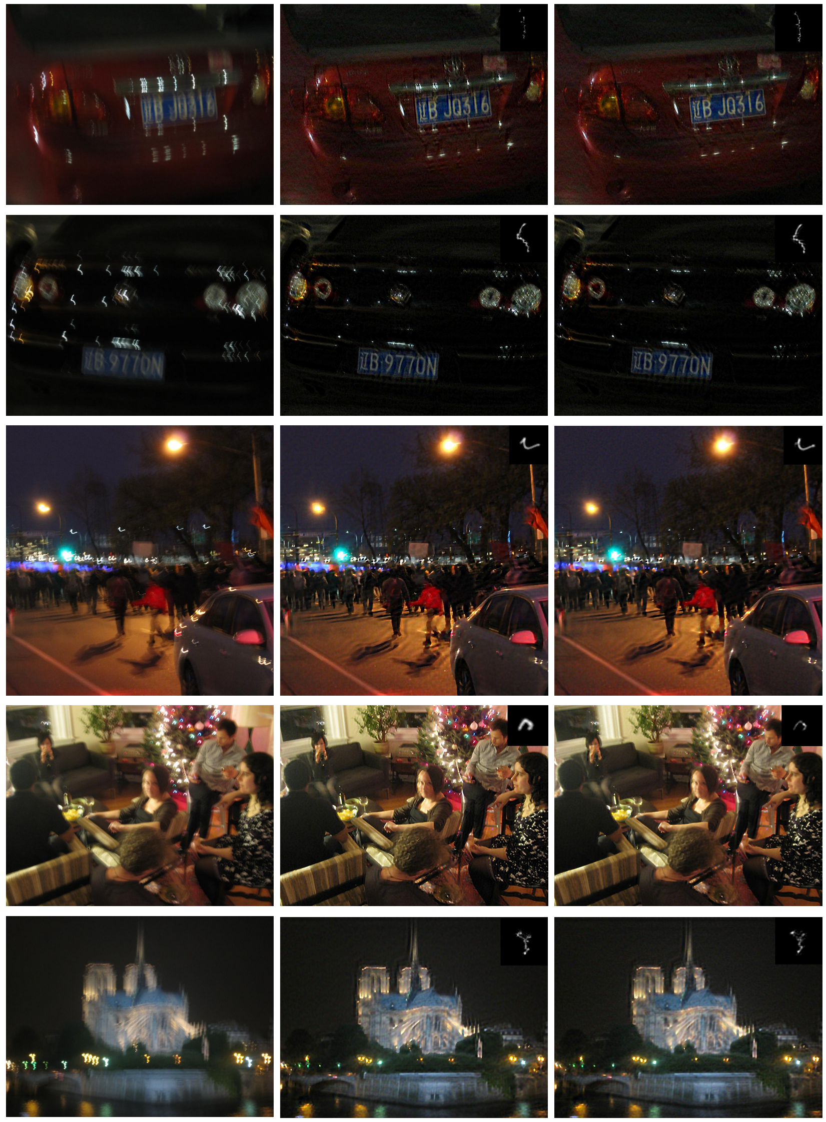

(a) Input (b) Hu et al. [7] (c) Ours

Fig. 21. Comparison with state-of-the-art methods on real-world saturated examples, OID performs comparable or even better than the method tailored to this scenario [7].

References

1. Chen, L., Fang, F., Wang, T., Zhang, G.: Blind image deblurring with local maximum gradient prior. In: IEEE CVPR (2019)
2. Cho, S., Lee, S.: Fast motion deblurring. ACM Transactions on Graphics **28**(5), 145 (2009)
3. Cho, S., Wang, J., Lee, S.: Handling outliers in non-blind image deconvolution. In: IEEE ICCV (2011)
4. Dong, J., Pan, J., Su, Z., Yang, M.H.: Blind image deblurring with outlier handling. In: IEEE ICCV (2017)
5. Fergus, R., Singh, B., Hertzmann, A., Roweis, S.T., Freeman, W.T.: Removing camera shake from a single photograph. ACM Transactions on Graphics **25**(3), 787–794 (2006)
6. Gong, D., Tan, M., Zhang, Y., van den Hengel, A., Shi, Q.: Self-paced kernel estimation for robust blind image deblurring. In: IEEE ICCV (2017)
7. Hu, Z., Cho, S., Wang, J., Yang, M.H.: Deblurring low-light images with light streaks. In: IEEE CVPR (2014)
8. Köhler, R., Hirsch, M., Mohler, B., Schölkopf, B., Harmeling, S.: Recording and playback of camera shake: Benchmarking blind deconvolution with a real-world database. In: ECCV (2012)
9. Krishnan, D., Tay, T., Fergus, R.: Blind deconvolution using a normalized sparsity measure. In: IEEE CVPR (2011)
10. Levin, A., Weiss, Y., Durand, F., Freeman, W.T.: Understanding and evaluating blind deconvolution algorithms. In: IEEE CVPR (2009)
11. Levin, A., Weiss, Y., Durand, F., Freeman, W.T.: Efficient marginal likelihood optimization in blind deconvolution. In: IEEE CVPR (2011)
12. Michaeli, T., Irani, M.: Blind deblurring using internal patch recurrence. In: ECCV (2014)
13. Pan, J., Hu, Z., Su, Z., Yang, M.H.: l_0-regularized intensity and gradient prior for deblurring text images and beyond. IEEE Transactions on Pattern Analysis and Machine Intelligence **39**(2), 342–355 (2017)
14. Pan, J., Lin, Z., Su, Z., Yang, M.H.: Robust kernel estimation with outliers handling for image deblurring. In: IEEE CVPR (2016)
15. Pan, J., Sun, D., Pfister, H., Yang, M.H.: Blind image deblurring using dark channel prior. In: IEEE CVPR (2016)
16. Shan, Q., Jia, J., Agarwala, A.: High-quality motion deblurring from a single image. ACM Transactions on Graphics **27**(3), 73 (2008)
17. Whyte, O., Sivic, J., Zisserman, A.: Deblurring shaken and partially saturated images. International Journal of Computer Vision **110**(2), 185–201 (2014)
18. Xu, L., Jia, J.: Two-phase kernel estimation for robust motion deblurring. In: ECCV (2010)
19. Xu, L., Zheng, S., Jia, J.: Unnatural l_0 sparse representation for natural image deblurring. In: IEEE CVPR (2013)
20. Yan, Y., Ren, W., Guo, Y., Wang, R., Cao, X.: Image deblurring via extreme channels prior. In: IEEE CVPR (2017)
21. Zhong, L., Cho, S., Metaxas, D., Paris, S., Wang, J.: Handling noise in single image deblurring using directional filters. In: IEEE CVPR (2013)